International Journal of Refrigeration 120 (2020) 39–49

Contents lists available at ScienceDirect

International Journal of Refrigeration

journal homepage: www.elsevier.com/locate/ijrefrig

A combined thermo-mechanical refrigeration system with isobaric expander-compressor unit powered by low grade heat – Design and analysis

Ahmad K. Sleiti*, Mohammed Al-Khawaja, Wahib A. Al-Ammari

Department of Mechanical and Industrial Engineering, College of Engineering, Qatar University, Doha, Qatar

ARTICLE INFO

Article history:
Received 12 June 2020
Revised 30 July 2020
Accepted 20 August 2020
Available online 24 August 2020

Keywords:
Thermo-mechanical refrigeration
Isobaric expansion engine
Refrigerants selection
Waste heat
VCR

ABSTRACT

Refrigeration and air conditioning systems consume about 17% of the world-wide electricity and their conventional refrigerants cause ozone depletion and global warming. In this study a novel thermo-mechanical refrigeration (TMR) system is developed and analyzed that is powered, instead of electricity, by thermal energy from waste heat or renewable sources in the ultra-low temperature range of 60–100 °C. A novel isobaric expander-compressor unit (ECU) is designed and combined with vapor compression refrigeration cycle to constitute the TMR system. The technological solutions (mainly towards simplification of the design) are crucial components of the study novelty. The suitable refrigerants for the system are systematically investigated, analyzed and selected from a list of 43 refrigerants. Nine fluids for the power loop (the isobaric expansion cycle) and nine fluids for the cooling loop (the thermal refrigeration cycle) were selected and compared based on their mode of operation (subcritical and supercritical), environmental effects and safety class. It is found that the HFO refrigerants such as R1234yf and R1234ze have acceptable performance with no ODP and very low GWP. Natural refrigerants R717 (ammonia) has the best performance in subcritical mode with toxicity as the main drawback. At heat source temperatures less than 85 °C, the system operation in subcritical mode is more efficient and more compact than in the supercritical mode. Thorough analysis and recommendations are made for the size of the ECU in terms of the diameters of the expander and the compressor.

Conception et analyse d'un système frigorifique thermo-mécanique combiné avec un groupe détendeur-compresseur isobare alimenté par une chaleur de faible qualité

Mots-clés: Froid thermo-mécanique; Machine à détente isobare; Choix des frigorigénes; Chaleur perdue; Froid à compression de vapeur

1. Introduction

It has been about 200 years since the vapor compression refrigeration cycle (VCRC) was invented. At that time, natural refrigerants such as ammonia, propane, and ether were used. Due to the flammability and toxicity of natural refrigerants, safe refrigerant families (chlorofluorocarbons (CFCs) and hydrochlorofluorocarbons (HCFC)) were introduced to replace the natural refrigerants through 1930s–1970s. However, it was discovered that these refrigerants cause ozone layer depletion. Then, alternative refrigerants (hydrofluorocarbons (HFCs)) that have zero Ozone Depletion Potential (ODP) with medium Global Worming Potential (GWP) were used. The continuous usage of the harmful refrigerants causes destructive environmental effects. This mandated researchers to develop new generation of refrigerants, HydroFluroOlefins (HFOs), which have zero ODP and very low GWP. In addition to that, the technological improvements and safety standards made it possible to use some natural refrigerants in refrigeration

* Corresponding author.
E-mail addresses: asleiti@knights.ucf.edu, asleiti@qu.edu.qa (A.K. Sleiti).

https://doi.org/10.1016/j.ijrefrig.2020.08.017
0140-7007/

Nomenclature

Symbol	Description, Units
A_c	cross-sectional area of the compressor piston, m^2
A_{ex}	cross-sectional area of the expander piston, m^2
D_c	diameter of the compressor piston, mm
D_{ex}	diameter of the expander piston, mm
h_1, h_2	specific enthalpy at the state point shown in Fig. 1, kJ/kg
L	the length of the power/backward stroke, mm
$\dot{m}_{cl}$	mass flow rate of the working fluid in the cooling loop, kg/s
$\dot{m}_{pl}$	mass flow rate of the working fluid in the power loop, kg/s
N	frequency of the expander-compressor unit (ECU), Hz
P_{c1}	saturated pressure in condenser 1, kPa
P_{c2}	saturated pressure in condenser 2, kPa
P_e	saturated pressure in the evaporator, kPa
P_h	pressure at the inlet of the heater, kPa
$\dot{Q}_e$	cooling capacity of the cooling loop, kW
$s_1, s_2,$	specific entropy at the states shown in Fig. 1, kJ/kg-°C
T_{c1}	condensing temperature of condenser 1, °C
T_{c2}	condensing temperature of condenser 2, °C
T_e	evaporator temperature, °C
T_h	heat source temperature, °C
v_3	specific volume of the working fluid at state 3 in Fig. 1, m^3/kg
$\dot{W}_c$	power consumed by the compression process, kW
$\dot{W}_{net}$	net power produced by the expander-compressor unit, kW
$\dot{W}_p$	power consumed by the pump, kW
η_{pl}	thermal efficiency of the power loop, %

Abbreviations

COP	coefficient of performance
CFC	Chlorofluorocarbons
ECU	expander-compressor unit.
GWP	global worming potential.
HCFC	Hydrochlorofluorocarbons.
HFC	Hydrofluorocarbons.
HFOs	hydrofluro-olefins.
ODP	ozone depletion potential.
ORC	organic Rankine cycle.
TMR	thermo-mechanical refrigeration system.
TDC	thermal-driven compressor.
VCRC	vapor compression refrigeration cycle.

applications (Danfoss 2012). In addition to the negative effects of the conventional refrigerants on the environment, refrigeration and air-conditioning systems consume about 17% (Naimaster and Sleiti, 2013; Sleiti and Naimaster, 2016) of the world-wide electricity and in the gulf countries, this percentage reaches alarming level of more than 67% (Sleiti et al., 2020), (Elbeih and Sleiti, 2020). This also contributes to the global warming since most of the grid-electricity is generated by conventional power plants that consume fossil fuels (Iir et al., 1963; Sleiti, 2017).

In recent decades, many researchers studied various options to create refrigeration systems that have no harmful effects on the environment (Sleiti et al., 2020). These systems could be classified into two major categories (based on the type of the energy source): a) electricity driven systems such as conventional Vapor Compression Cycle (VCC) driven by PV panels (Lazzarin, 2014), or thermoelectric cooling (Söylemez et al., 2018), b) heat-driven systems driven by thermal energy sources (solar, geothermal, waste heat). The latter category is classified into: a) sorption-process systems (such as absorption refrigeration systems (Berdasco et al., 2019), adsorption refrigeration systems (Habib et al., 2011)) and b) thermal mechanical refrigeration systems (such as VCC systems driven by ORC (Jeong and Kang, 2004) and ejector refrigeration systems (Rostamnejad and Zare, 2019). Other systems that combine both thermal and electrical refrigeration, simultaneously are suggested in Salhi et al. (2018) and Khaliq (2015). Each of these systems has its advantages and disadvantages based on the application, heat source type, capacity of the system and other factors. For instance, the VCC powered by PV cell is considered as an attractive option in countries that have high solar radiation intensity (Sleiti et al., 2020). However, the cost of their batteries still very high (Zeyghami et al., 2015). The application of ORC is not economical at heat source temperatures lower than 100 °C (Sleiti et al., 2020). Absorption system does not work efficiently at temperatures less than 90 °C. Due to the simplicity of the ejector structure, numerous studies have been presented to improve its COP and its operation stability at off-design conditions (Shestopalov et al., 2015; Shestopalov et al., 2015). The improvement approaches of the ejector and ORC where reviewed comprehensively by Sleiti et al. (2020). The improvement approaches of the ejector systems include its improvement as component (by improving its geometry (Van Nguyen et al., 2020; Yan et al., 2016; Wu et al., 2014; Foroozesh et al., 2020)), operating mechanism (Dennis and Garzoli, 2011; Zhu et al., 2014), working fluids (Roman and Hernandez, 2011; Nemati et al., 2017) and operating conditions (Chen et al., 2017)), as a system (such as bi-ejector system (Yu and Li, 2007) and free-pump ejector systems (Srisastra et al., 2008)), and as an integrated system (with power cycles and/or with other cooling cycles (Sanaye and Refahi, 2020; Sioud et al., 2019; Heidari et al., 2019). Similarly, the ORC improvement approaches introduced by the development of the cycle itself (by improving the expander efficiency (Ziviani et al., 2018), and working fluids selection (Frutiger et al., 2016)) and by the integration with other power or cooling cycles (Sleiti et al., 2020).

A new approach for building refrigeration systems powered by ultra-low heat temperature sources was presented by Sleiti et al. (2018) based on the work developed by Encontech BV Glushenkov et al. (2018). They proposed the integration of the conventional VCC with isobaric compressor, namely Bush compressor and the whole system is referred to as Thermo-Mechanical Refrigeration (TMR) system. The compressor works by means of an isobaric expansion engine (engines that produced work by expansion process at constant pressure). The concept of using isobaric expansion to convert thermal energy to mechanical energy is not new. However, the related problems to its application in actual systems still in the research phase. In 1841, another technology; direct-acting steam pump was invented by Henry Worthington (ASME, 2016), see Glushenkov et al. (2018) for more details on potential applications. It consists of steam and pumping cylinders with rigidly-connected steam and pumping pistons inside them. Each cylinder has two control valves. As the inlet valve of the steam cylinder is opened, the steam piston moves and compresses the liquid in the pumping cylinder. That is, the isobaric expansion of the steam performs the compression of the liquid pump. At the end of the expansion stroke, the inlet steam valve closes, and the outlet valve opens. By the pressure of the liquid entering the liquid cylinder, the steam piston moves back, and the reciprocating motion then repeats. This pump is still being used in applications such as boiler feed pumps, ship emergency pumps without any significant changes in the original design. The operation principle of this pump could be used to generate mechanical energy from thermal energy (like the Worthington pump-based power plant producing shaft power proposed by Glushenkov et al. (2018). The principle of

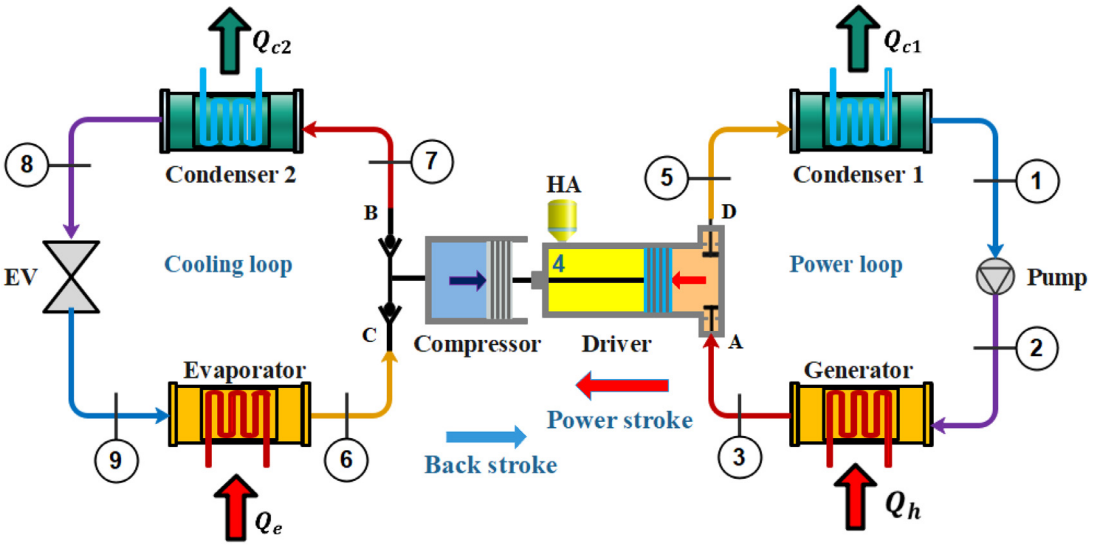

Fig. 1. Schematic diagram of the TMR system.

the isobaric expansion was also implemented to build Bush compressor. The main feature of this compressor is its ability to directly convert thermal energy to mechanical energy used to perform a compression process. Also, in some advanced versions, it could be made as a self-oscillating piston to eliminate the sealing and its related losses. However, the sensitivity to dead volumes and the low thermal expansion of gases are considered as the main drawbacks of the Bush compressor.

The selection of the working fluids for power and refrigeration cycles play major role in their performance, size, and cost (Duarte et al., 2019). Many researchers studied the performance of various working fluids in thermal refrigeration systems. However, the recommended fluids differ according to the main objectives of these studies. In the present study, we intend to select the proper refrigerants that could be used in a thermo-mechanical refrigeration system powered by ultra-low heat temperature sources in the range of (60–100 °C). This system uses the isobaric expansion principle to drive the compressor of the conventional vapor-compression refrigeration cycle. The authors of the current paper conducted a detailed review in Sleiti et al. (2020) of thermo-mechanical refrigeration systems including ejector, ORC, and isobaric expansion systems. Only one study was found in open literature by Aphornratana and Sriveerakul (2010) that has studied the performance of a thermal refrigeration system, however they studied only two working fluids (R22 and R134a) in subcritical mode. Furthermore, they performed calculations by applying isentropic relations that are only valid for ideal gases. In contrast, in the current work, all refrigerants in EES program library have been analyzed and the selection of the fluids is performed in a systematic method. In addition to that, the present work introduces a comparison between subcritical and supercritical operation modes of the power cycle, not studied before in open literature.

The novelty aspects of the current study can be summarized as follows: (i) the TMR in the current study is designed to work on low heat temperature sources with no complex processes nor high maintenance requirements, unlike existing ORC and its variations; (ii) the thermodynamic cycle of the heat driven compressor with suitable working fluids as in the current study have never been used in heat engines; (iii) the technological solutions (mainly towards simplification of the design) are crucial components of the study novelty and (iv) a comparison is provided between subcritical and supercritical operation modes of the power cycle, not studied before in open literature.

The present study is subdivided into 5 sections. Section 2 describes the operating mechanism of the TMR system and its components in addition to the specifics of the expander-compressor unit design. Section 3 presents the thermodynamic model of the TMR system. Section 4 discusses the working fluid selection process, simulation of the subcritical mode of the system with design and environmental parameters, and comparison between subcritical and supercritical operation modes of the system.

2. TMR system description

Fig. 1 shows the proposed thermal mechanical refrigeration system (TMR). It consists of vapor compression refrigeration system with replacing the electrically powered compressor by a low-grade thermal powered compressor (TPC).

The compressor power is provided by an isobaric expander. The expander-compressor unit (ECU) consists of two cylinders with two connected pistons, details of which are provided in Section 2.1 below. The expander power is supplied by the expansion of high-pressure vapor generated in the heater. The heater receives heat from low-grade waste heat. The working fluid is to be an organic fluid such that the generation of high-pressure vapor is achieved with low-grade heat sources (with temperatures less than 100 °C).

The overall operation of the system could be explained as follows: in the power stroke, the saturated liquid of the working fluid at the condenser pressure (point 1) is pumped by the isentropic pump to the heater pressure (point 2). The high-pressure fluid flows into the heater and evaporates to saturated vapor state then directed to the expander (point 3). The vapor that enters the expander through valve A undergoes an isobaric expansion process by displacing the piston to the left direction. During the expansion, the refrigerant inside the compressor is compressed to the high pressure, P_h, which is the condenser pressure (condenser 2) and discharged through valve B (point 7). The cooling refrigerant is condensed by condenser 2 (process 7–8) then throttled to the evaporator (process 8–9) to produce the cooling effect. Then it flows back into the compressor cylinder through valve C (point 9) to perform the back stroke. At the same instant, valve D is opened to discharge the working fluid of the expander to condenser 1. Valve D acts as a throttling valve so the pressure through the discharging process drops from the heater pressure to condenser pressure (point 5). The backstroke of the expander cylinder can be performed by the evaporator pressure and pneumatic mechanism

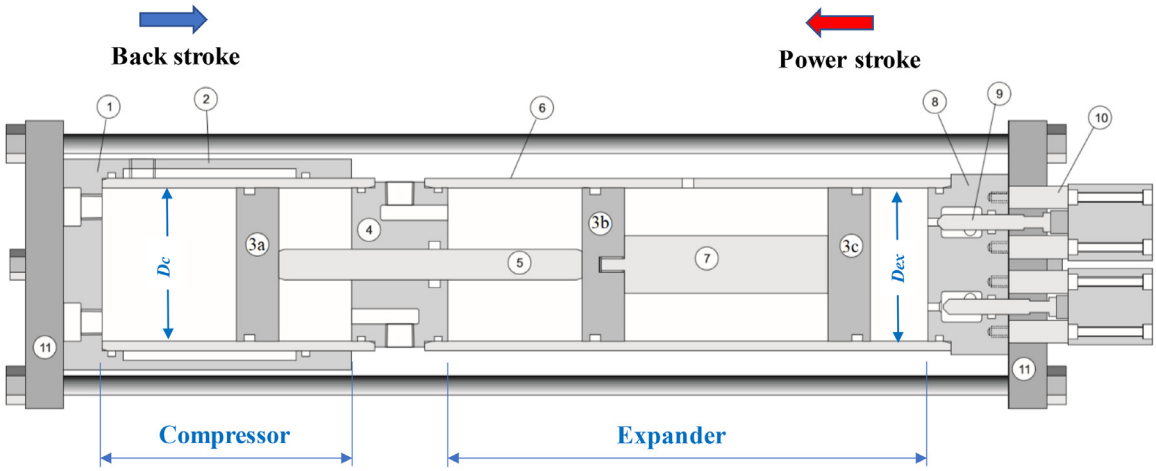

Fig. 2. Expander-compressor unit. (1) cooling jacket, (2) compressor cylinder, (3) pistons, (4) auxiliary cover, (5) rod, (6) expander cylinder, (7) expander piston, (8) valve cover, (9) valve stem, (10) pillar, (11) flange.

(not shown in Fig. 1). Alternatively, the valve mechanism could be adjusted such that the high pressure of the power loop performs both the power stroke and the backward stroke (double acting piston as those used in Westinghouse steam driven air compressor). After condenser 1, the expander working fluid is condensed to the saturated liquid state (point 1). Then the cycle is repeated. The control process of valves A and D is usually performed by electrical, hydraulic or pneumatic actuators to ensure precise opening and closing of the valves during the expansion (power) and back strokes. For instance, (based on the design, operating conditions and safety requirements) one can use single/double pilot pneumatic valve to fill and empty the cylinder chamber with the aid of mechanical spring or accumulator (see the operating mechanism and the connection method by Airmax Pneumatics LTD (2020).

2.1. Design of the isobaric expander-compressor unit (ECU)

The detailed design of the ECU, which is schematically shown in Fig. 1, is provided in Fig. 2. The ECU performs two strokes; the stroke from right to left referred to as the compression stroke and from left to right referred to as expansion stroke. In the compression stroke, the working fluid that is coming from the power loop (at state 3 in Fig. 1) enters the right-hand chamber of the expander cylinder (6) via valve stem (9). The valve stem is a self-contained valve that opens to admit the working fluid to the first chamber of the expander cylinder (6) and is then automatically closed and kept sealed by the pressure in the chamber. Due to the rise of the pressure in this chamber, the expander piston (3c) moves to the left along with expander piston (7), expander piston (3b), rod (5) and compressor piston (3a). The compressed working fluid in cylinder 3, enters the cooling loop via the non-return valve (B) shown in Fig. 1 to perform the cooling cycle (states 7-8-9-6 in Fig. 1).

In the back stroke, the working fluid enters cylinder (2) via the non-return valve (C), shown in Fig. 1, causing piston (3a), rod (5), pistons (3b), (7) and (3c) to move from left to right. The working fluid now exits the ECU via valve stem (9) and flows back to the power loop shown in Fig. 1 to complete the power cycle (states 5-1-2-3 of the power loop).

The novel ECU design presented in Fig. 2 and the TMR system proposed in the current study are based on the use of innovative prime mover (heat engine acting as compressor, Fig. 2) that can be combined with vapor compression refrigeration. The prime mover can be positioned in between ORC engines and Stirling-cycle thermal machines. The thermodynamic cycle of the heat driven compressor with suitable working fluids as in the current study have never been used in heat engines. The technological solutions (mainly towards simplification of the design) are crucial components of the study novelty.

The Organic Rankine Cycle (ORC) is the only proven and industrially applied technology to convert low-temperature heat into power. It is considered to be the most efficient and economic technology in temperature ranges of 200–400 °C (Bianchi and De Pascale, 2011). An assessment of the potential of various heat recovery technologies by Hammond and Norman (2014) showed that the greatest potential for reusing the surplus heat available is, in particular, in conversion to electricity, mostly using ORC technology. However the specific costs of 2000–4000 €/kW (Heberle and Brüggemann, 2015) is rather high. At ultra-low heat source temperatures, below 100 °C, the technology is not economic at all. The Kalina cycle, a variation of the classical ORC utilizing water-ammonia mixtures, is a promising alternative for very low temperature sources. However, studies indicate that the promised benefits of Kalina cycles appear over-estimated while this process is much more complex and maintenance demanding than classical ORC processes (Chen et al., 2010). In contrast to ORC and its variation, the TMR in the current study is designed to work on low heat temperature sources with no complex processes nor high maintenance requirements.

3. Thermodynamic modeling

Throughout the modeling of the TMR system, the following assumptions were made:

1 The changes in kinetic and potential energies are neglected.
2 The pressure drop through the connecting pipes is neglected (Aphornratana and Sriveerakul, 2010).
3 All pipes and Expander/compressor cylinders are well insulated.
4 The working fluid of the power loop leaves the heater as saturated vapor.
5 The compression process (6–7) is performed isentropically (Aphornratana and Sriveerakul, 2010).

Starting with pumping process from point 1 to point 2 (see Figs. 1 and 3), the consumed power by the pump is given as (Cengel and Boles, 2015):

$$\dot{W}_p = \dot{m}_{pl}(h_2 - h_1) \quad (1)$$

where $\dot{m}_{pl}$ is the fluid mass flow rate of the power loop. The enthalpy at point 1 (h_1) is obtained at the saturation temperature

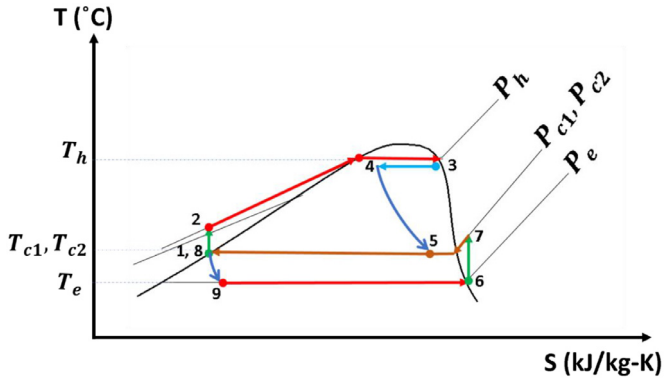

Fig. 3. T-S diagram of the TMR system (for the same working fluid in both loops).

T_{c1} and quality of $x_1 = 0$. Assuming that the pump process (1–2) is isentropic, the enthalpy at point 2 is obtained at heater pressure P_h and entropy $s_2 = s_1$. The required power to evaporate the working fluid inside the heater from point 2 to 3 is given as (Cengel and Boles, 2015):

$$\dot{Q}_h = \dot{m}_{pl}(h_3 - h_2) \tag{2}$$

where the enthalpy at point 3 is obtained at the heater pressure P_h and quality of $x_3 = 1$ (saturated vapor).

Referring to Figs. 1 and 3, the produced power by the expander through the expansion process (point 3 to 4) is calculated as (Glushenkov et al., 2018; HYPERLINK \l "bib47" Cengel and Boles, 2015):

$$\dot{W}_{ex} = \dot{m}_{pl}(h_3 - h_4) \tag{3}$$

$$\dot{W}_{ex} = NLA_{ex}(P_h - P_{c1}) \tag{4}$$

where N is the frequency of the cycle, L is the length of the stroke and A_{ex} is the cross-sectional area of the expander piston.

The power produced by the expander is directly consumed by the compressor, that is:

$$\dot{W}_{net} = W_{ex} - W_p \tag{5}$$

$$\dot{W}_{net} = \dot{W}_c \tag{6}$$

Also, the compressor power $\dot{W}_c$ is given as:

$$\dot{W}_c = \dot{m}_{cl}(h_7 - h_6) \tag{7}$$

where $\dot{m}_{cl}$ is the fluid mass flow rate inside the cooling loop. The enthalpy h_6 is obtained at the evaporator pressure P_e and quality $x_6 = 1$. The enthalpy h_7 is obtained at the condenser pressure P_{c2} and entropy of $s_7 = s_6$ (by the assumption # 6). The cooling capacity of the evaporator is given as:

$$\dot{Q}_e = \dot{m}_{cl}(h_6 - h_9) \tag{8}$$

Table 1
Range of the input parameters.

Parameter	Range	unit
High cycle temperature of the power loop, T_h	60–100	°C
Low cycle temperature of the power loop, T_{c1}	30–50	°C
High cycle temperature of the cooling loop, T_{c2}	30–50	°C
Low cycle temperature of the cooling loop, T_e	-10–5	°C
Cooling capacity of the evaporator, $\dot{Q}_e$	1 (design capacity)	kW
Length of the expansion stroke, L	5–15	cm
Frequency of the cycle, N	0.5–5	Hz

where enthalpy h_9 is equal to h_8, which is obtained at the condenser pressure P_{c2} and quality of $x_8 = 0$.

The mass flow rate of the power loop is given as:

$$\dot{m}_{pl} = \frac{NLA_{ex}}{v_3} \tag{9}$$

where v_3 is the specific volume of expander working fluid at point 3 (at the inlet of the expander).

$$A_{ex} = \pi D_{ex}^2/4 \tag{10}$$

Also, the mass flow rate of the cooling loop is given as:

$$\dot{m}_{pl} = \frac{NLA_c}{v_6} \tag{11}$$

where Ac is the cross-sectional area of the compressor piston given as:

$$A_c = \pi D_c^2/4 \tag{12}$$

and v_6 is the specific volume of the cooling fluid at point 6 (at the inlet of the compressor).

The efficiency of the power loop is given as:

$$\eta_{pl} = 100 \times \frac{\dot{W}_{net}}{\dot{Q}_h} \tag{13}$$

The Coefficient of Performance (COP) of the cooling loop is expressed as:

$$COP = \frac{\dot{Q}_e}{\dot{W}_c} \tag{14}$$

where $\dot{W}_c = W_{ex} - W_p$ as defined by Eqs. (5) and (6) above.

The flowchart of the calculation process is shown by Fig. 4 and the input parameters are given in Table 1. The simulation process of the system with several working fluids was performed using Engineering Equation Solver (EES). The range of the operating conditions was selected based on the nominal climate conditions of Qatar and the desired temperature range of the low-grade thermal sources. Also, the range of the cycle frequency is slower than the commercial compressors to avoid technical problem such as wearing, noise, and overheating of the piston. Furthermore, low frequency implies that the lifetime of the ECU is longer than the conventional compressors.

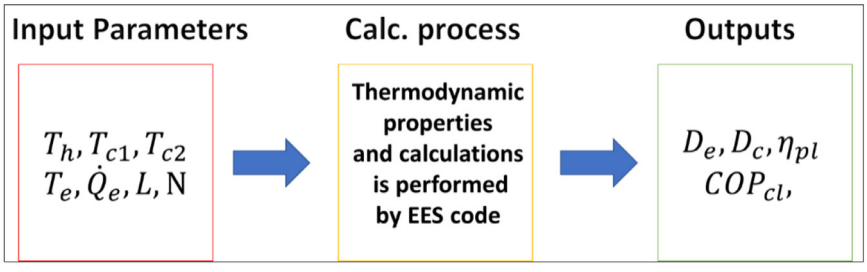

Fig. 4. Flowchart of the calculation process.

Table 2
Model verification.

	Fluid	L mm	D_{ex} mm	D_c mm	N Hz	T_h °C	T_{c1}, T_{c1} °C	T_e °C	Q_e kW	Q_h kW	Area ratio A_{comp}/A_{ex}	Overall COP
Ref. (Aphornratana and Sriveerakul, 2010)	R134a	150	29.13	50.50	1	80	35	5	0.75	3.0	3.00	0.274
Present work	R134a	150	29.39	49.40	1	80	35	5	0.75	2.8	2.82	0.270
Diff.%	–	0	0.89	2.28	0	0	0	0	0.00	6.1	6.00	1.5

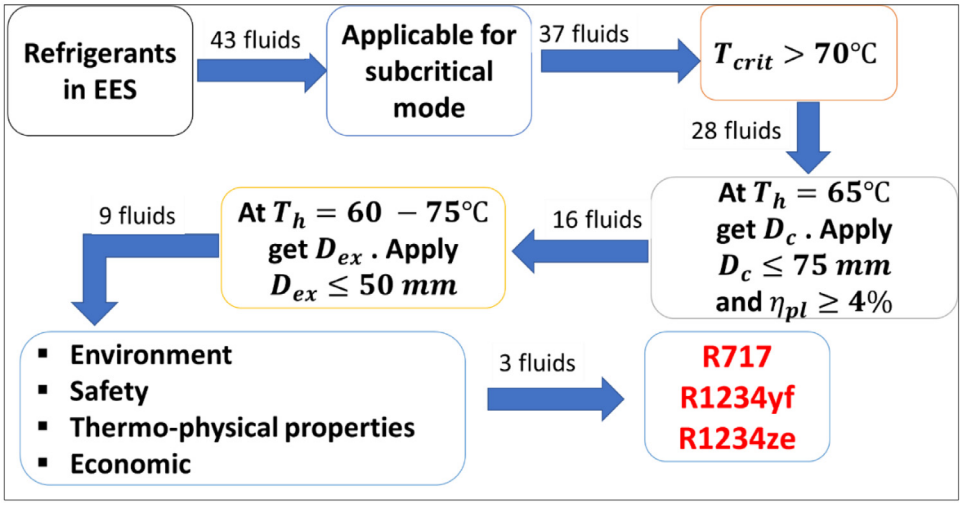

Fig. 5. Steps of working fluid selection of the power loop of the TMR system.

4. Results and discussion

4.1. Model verification

To verify the model of the TMR system, a comparison was made between the results of this model and those obtained by the only study found in literature with similar objective (but different design, assumptions and approach) by Aphornratana and Sriveerakul (2010). See discussion in the introduction section above about the work presented in Aphornratana and Sriveerakul (2010) and how it is different from the current study. As shown in Table 2, at the same input conditions and same working fluid, R134a, the obtained expander and compressor diameters of the present model are very close to that used by the published model. It should be noted that Aphornratana and Sriveerakul (2010) have defined the compressor diameter as an input and the cooling capacity as an output. In this paper, the inverse is done; we define the required cooling capacity to obtain the required diameters that satisfy it. Also, they obtained the thermodynamics properties from ASHRAE while the present work uses EES library.

4.2. Selection criteria of the working fluids

There are several factors that affect the selection process of the proper working fluids such as energy efficiency, system size, safety, environmental effects, thermo-physical properties and the availability and cost of the fluids. There is no ideal criteria to select a fluid that satisfies all the design requirements, so tradeoffs have to be made. For instance, some fluids have attractive performance but have negative effects on the environment or their cost is very high relative to other fluids. Other fluids may have eco-friendly use, but their performance is not efficient. In the present TMR system, to select proper working fluids, specific criteria were applied to the available refrigerants in EES program (43 fluids). These criteria are discussed in this section.

Fig. 5 shows the steps of working fluid selection of the power loop of the TMR system. Through the selection process, the input data were set as: $Q_e = 1$ kW, $L = 50$ mm, $N = 5$ Hz, $T_{c1} = T_{c2} = 40$ °C, and $T_e = -5$ °C. First, the selection process was applied to 43 working fluids available in EES. Then, the refrigerants that have variable saturation pressure (mixtures) were eliminated. The range of interest of the heat source temperature is from 60 to 100 °C, so refrigerants with critical temperature lower than 70 °C were also eliminated (9 fluids).

The remaining 28 fluids were simulated at heat source temperature of 65 °C. To ensure suitable performance and small size of the isobaric expander-compressor unit, the fluids that require compressor diameter higher than 75 mm or produced power with efficiency of power loop less than 4% were eliminated (12 fluids). The simulation process is repeated with larger range of heat source temperature (60–75 °C). In this case, the fluids that require expander diameter higher than 50 mm were eliminated (7 fluids). Now, the 9 remaining fluids were compared to each other based on their environmental effects (GWP, ODP, and lifetime in atmosphere), safety class, and their thermo-physical properties as shown in Table 3. The power loop efficiency associated with the 9 selected fluids in Table 3 is shown in Fig. 6 for the same working fluid in booth loops over the heat source temperature range of 60–100 °C. It can be noted that R717 (Ammonia) has the highest power loop efficiency (max. 7.5%), while R1234yf has the lowest efficiency (min. 4%). The other 7 fluids have similar efficiencies with optimum obtained at 83–87 °C.

Referring to Table 3, R12 and R500 are CFC refrigerants, which have high global warming potential and ozone depletion potential. Furthermore, they are phased out refrigerants. So, R12 and R500 are eliminated from selected fluids list. Also, from the safety point of view, R161 and R290 have safety class of A3. That means these refrigerants have high flammability. Taking into account that HFO refrigerants have low GWP relative to their HFC alternatives, R1234yf and R1234ze are selected as proper working fluids for the power loop of the presented TMR system. R717 (ammonia) has no GWP or ODP with lowest atmospheric life and highest efficiency. The main drawback of R717 is its toxicity nature. However, it is widely used in commercial refrigeration applications due to its low

Table 3
Comparison of the 9 selected fluids for the power loop. Properties were obtained at optimum performance temperature of 83 °C.

Fluid	Critical temp. T_{cr} °C	Critical pressure P_{cr} kPa	Enthalpy h kJ/kg	Specific volume v $\frac{kg}{m^3} \times 10^{-3}$	GWP	ODP	Atm life (yrs.)	Safety class	Toxicity class	Category
R717	132.3	11,333	1471.0	27.40	0	0	0.010	B2L	B	Natural
R161	102.1	5010	600.5	9.03	12	0	0.210	A3		HFC
R290	96.7	4247	627.8	10.79	20	0	0.041	A3	A	HC
R152a	113.3	4520	543.1	11.25	138	0	1.400	A2	A	
R1234yf	94.7	3382	398.1	4.99	4	0	0.029	A2L	A	HFO
R143m	104.8	3635	437.6	7.34		0				HFC
R500	105.5	4455	249.3	6.11	8077	0.66	0.731	A1		CFC
R12	112.4	4114	213.0	6.33	10,890	1	100.00	A1		CFC
R1234ze	109.4	3632	427.9	7.41	6	0		A2L	A	HFO

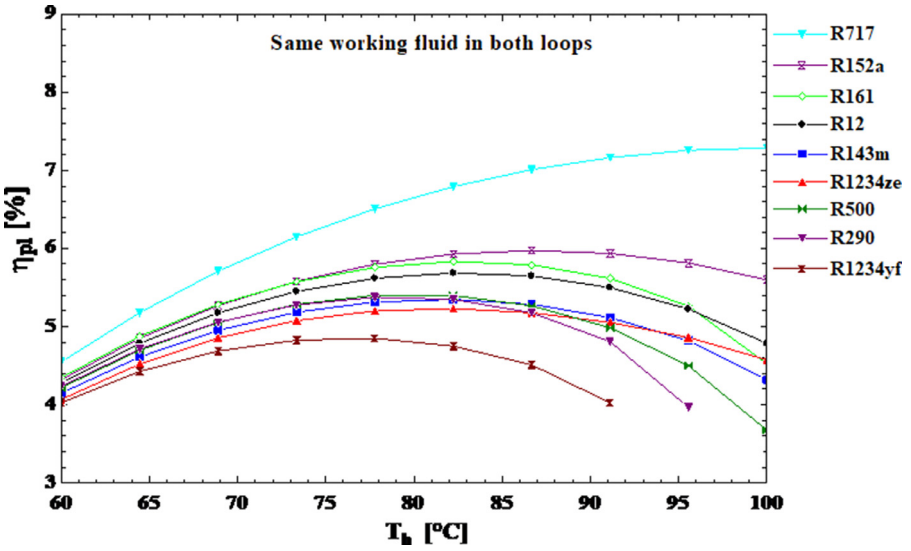

Fig. 6. Power loop efficiency of the 9 selected fluids within the design heat source temperature range.

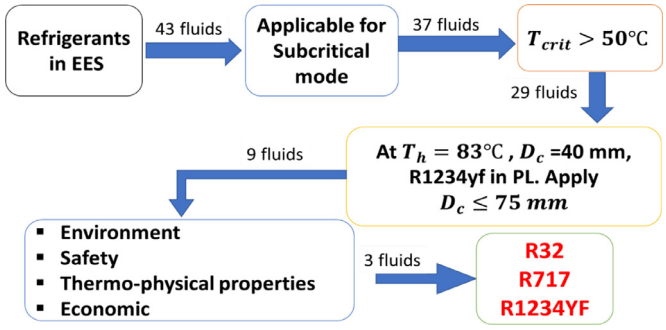

Fig. 7. Steps of working fluid selection of the cooling loop of the TMR system.

cost and good performance. So, it is selected as a suitable working fluid for the TMR system.

Similar to the process of the working fluid selection of the power loop, Fig. 7 shows the selection steps of the working fluid of the cooling loop. However, in this process, all the fluids with critical temperature less than 50 °C were eliminated. This is done because the condensing temperatures are usually between 30 and 45 °C in regions of interest such as in Qatar. It was found that there are 9 selected fluids (shown in Fig. 8) that showed attractive performance in the cooling loop. As for the power loop, R12 and R502 are phased out refrigerants, so they are eliminated from further analysis. As shown in Table 4, R32 has a medium GWP while R13B1 and R143a have high GWP. So, for safety and environmental purposes, R13B1, R143a, R161, and R290 were considered as alternative working fluids for the cooling loop. R717, R1234yf, and R32 are the best selected fluids of the cooling loop for their high Q_e and thus COP (see Fig. 8) and acceptable environmental properties.

4.3. Performance in the subcritical mode

In the present research work, subcritical mode refers to the state of the working fluid at the inlet of the expander that is not supercritical or superheated. It is a saturated vapor corresponding to the saturation temperature of the heat source. The efficiency of the power loop, COP of the cooling loop and the diameters of the expander and the compressor are considered as performance indicators (PIs). The performance of the system varies with the variation of the operating conditions such as the heat source temperature, condenser temperature and evaporator temperature. In this section, R717 is used as the working fluid of the power loop and R32 is the working fluid of the cooling loop as these two fluids together provide better performance in subcritical mode.

Fig. 9(a) shows the variation of the power loop efficiency with the heat source temperature. It can be noted that higher source temperature increases the efficiency up to an optimum point. At 60 °C, the power efficiency is 4.5%, which is 75% of Carnot efficiency. At 100 °C, the power efficiency is 7.2%, which is 44.8% of Carnot efficiency. Further increase of the heat source temperature reduces the efficiency. Also, higher source temperature provides higher pressure at the inlet of the expander, which minimizes the required diameters of the expander and compressor pistons as shown in Fig. 9(a) and (c). In addition to that, the increase of the cooling capacity increases the required diameters of the expander and compressor pistons with no effect on the efficiency of the power loop. At cooling capacity of 1 kW and heat source

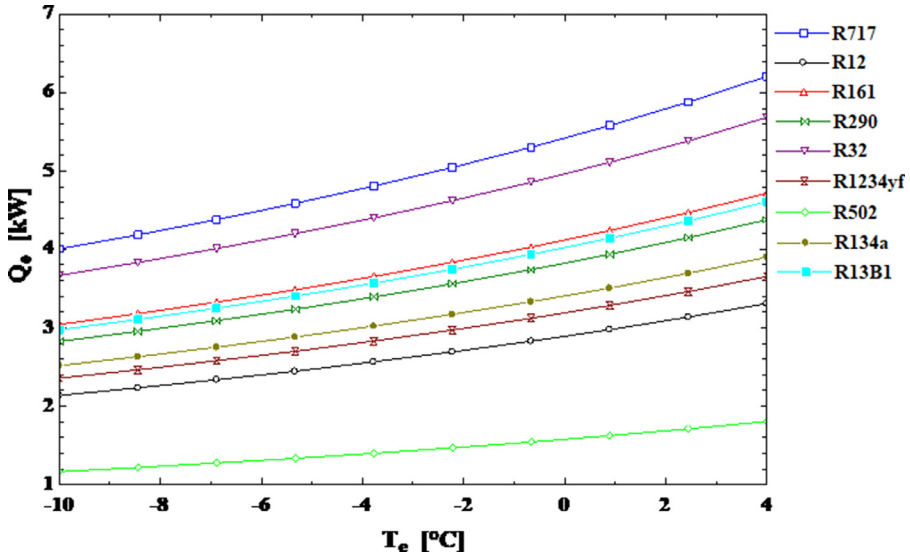

Fig. 8. Cooling capacity of the 9 selected fluids of the cooling loop within the design range of the evaporator temperature.

Table 4
Selected fluids of the cooling loop. Properties were obtained at – 5 °C.

Fluid	Critical temp.T_{cr}°C	Critical pressure P_{cr} kPa	Enthalpy h kJ/kg	Specific volume v $\frac{kg}{m^3}$ $\times 10^{-3}$	GWP	ODP	Atm life (yrs.)	Safety class	Toxicity class	Category
R32	78.1	5784	514.3	53.3	675	0		A2L		
R13B1	67.0	3971	122.6	17.4	7140	16	65	A1		
R143a	72.7	3761	385.2	42.9	4470	0	52	A2		
R717	132.3	11,333	1457.0	346.5	0	0	0.01	B2L	B	Natural
R161	102.1	5010	575.3	114.8	12		0.21	A3		HFC
R290	96.7	4247	569.1	112.1	20		0.041	A3	A	HC
R1234yf	94.7	3382	360.0	66.8	4	0	0.029	A2L	A	HFO

Table 5
Comparison of the thermo-mechanical refrigeration system (TMR) with other cooling technologies (Sleiti et al., 2020).

Technology	Heat source temperature, °C	COP	Main Advantages	Main Limitations
Electricity driven cooling (PV, TEC)	–	3–3.45	Flexible and reliable	High cost
Absorption	85–220	0.7–1.25	High cooling capacities	Limited operating temperature
Adsorption	60–165	0.3–0.7	Less corrosion at high temperatures	Expensive and bulky systems
Desiccant	60–95	0.3–0.51	Low operating temperatures	Complex control, crystallization risk
ORC	100–300	0.1–0.75	A mature technology	Not economical at temperatures lower than 100°C
Ejector	60–160	0.1–0.62	Simple, high capacity	Not flexible
TMR	60–100	1.2–2.6	Simple, flexible	Low cooling capacities,

temperature of 60 °C, the required expander and compressors diameters are 72.6 and 75.4 mm, respectively. At heat source temperature of 100 °C, the required diameters are 34.5 and 74.4 mm, respectively. This means that the increase of the heat source temperature from 60 to 100 °C, reduces the expander diameter by 52.5% with the same compressor diameter. The compressor diameter is mainly affected by the parameters of the cooling loop such as cooling capacity, evaporator temperature and condenser temperature. For instance, at cooling capacity of 1 kW, the compressor diameter is 75.4 mm, while at 5 kW it is 168.6 mm. Also, higher cooling capacity requires higher expander diameter (as shown in Fig. 9(a)). The required expander diameter at 5 kW cooling capacity is at least two times higher than at 1 kW cooling capacity.

As shown in Fig. 9(b) and (c), the condenser temperature has considerable effect on the performance of the power and cooling loops. The range of the condensing temperature is selected to be 30–50 °C to ensure the occurrence of the condensation process for both average and high temperature regions. Higher condenser temperature requires higher pressure in the condenser, which increases the load of the compressor. Fig. 9(c) reveals that the increase of the condensation temperature from 30 to 50 °C increases the required diameter of the expander piston by more than 60% with less than 1% increase in the compressor piston diameter. This is explained by that the compressor diameter is a function of the cooling capacity, while the expander diameter is a function of the work rate of the compressor. Also, it can be noted that the power loop efficiency is not affected by the increase of the cooling capacity. At condensing temperature of 50 °C and cooling capacity of 1 kW, the power efficiency is 6% with expander and compressor diameters of 92.50 and 75 mm, respectively. At the same temperature with cooling capacity of 5 kW, the power efficiency is 6% with expander and compressor diameters of 210 and 180 mm, respectively.

The evaporator temperature also has considerable effect on the size of the expander and compressor diameters, Fig. 9(d). At the same cooling capacity, lower evaporator temperature, minimizes the pressure at the inlet of the compressor. This in turn requires higher compressor power with larger diameters. However, the increase of the expander and compressor diameters is not significant compared to the increase of the condenser temperature. For instance, at cooling capacity of 1 kW and evaporator temperature of −5 °C, the expander and compressor diameters are 68 and 72 mm, respectively. At the same capacity with evaporator temper-

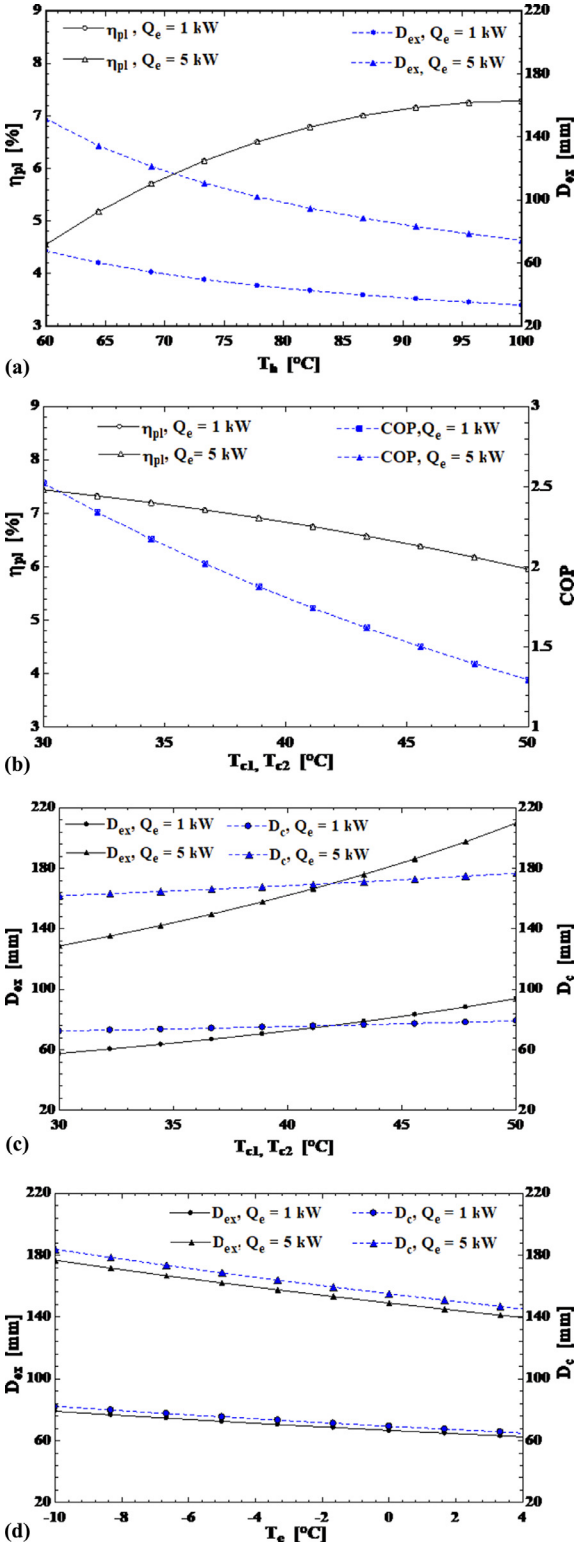

Fig. 9. Performance of the subcritical mode. a) heat source temperature with power loop efficiency, b) condenser temperature with power loop efficiency and COP of the cooling loop, c) condenser temperature with expander and compressor diameters, and d) evaporator temperature with expander and compressor diameters.

ature of −10 °C, the compressor and expander diameters are 80 and 84 mm.

The COP results of the TMR system of the present study are compared to the results of typical refrigeration systems reviewed by Sleiti et al. (2020) as shown in Table 5. The TMR system has

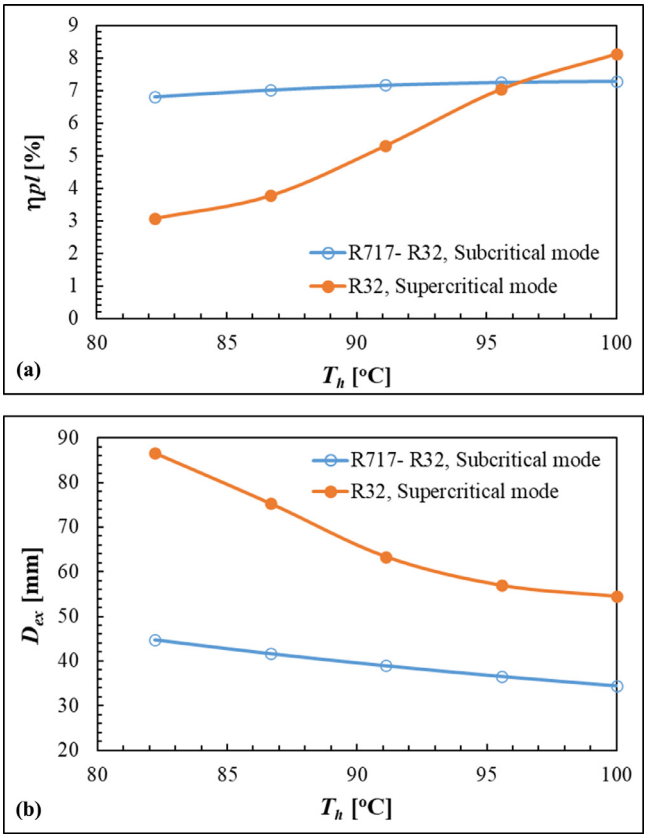

Fig. 10. Performance of the supercritical mode. (a) heat source temperature with power loop efficiency of subcritical and supercritical modes, and (b) heat source temperature with the expander diameter of the subcritical and supercritical modes.

better COP (1.2–2.6) than other thermal driven systems with simple and flexible design. The low cooling capacity limitation of the TMR system can be mitigated by installing several systems in parallel to boost the cooling capacity.

4.4. Performance in the supercritical mode

Supercritical mode refers to the state of the working fluid that is supercritical at the entrance of the expander. In this mode, it is found that R32 has the best performance over the other refrigerants in EES. Compared to the best case of the subcritical mode, where R717 in power loop with R32 in cooling loop performed best, in the supercritical mode, however R32 in both loops showed best performance. Elaboration on this is provided next.

At high cycle temperature (T_h) of less than 85 °C, (see Fig. 10(a)), the power efficiency in the subcritical mode is two to three times higher than that in the supercritical mode. This is explained by that R717 consumes less pumping power in subcritical mode than R32 in supercritical mode.

Also, the required heat to be supplied by the heater, reduces with the increase of the heat source temperature in subcritical mode, while it increases in supercritical mode. The required expander and compressor diameters in supercritical case are larger than that of the subcritical mode case. This is because R32 has higher pressure in both loops, which requires more work rate and so larger piston diameter. Also, at higher source temperature, the required diameter becomes closer in both modes (see Fig. 10(b)). In addition to that, at heat source temperature larger than 95 °C, the supercritical mode is more efficient and closer in size to the subcritical mode. This is due to the increase of the pumping power with temperature increase in subcritical mode, while pumping

power in supercritical mode is not a function of the heat source temperature.

5. Conclusions

In this research study, a novel thermo-mechanical refrigeration (TMR) system is developed and suitable refrigerants as working fluids for the system are selected and recommended. The TMR system consists of an isobaric-exposition engine powered by ultra-low heat source temperature and used to directly drive a vapor compression refrigeration cycle. The selection of the working fluids is performed systematically according to strict criteria and a number of design factors including the performance, size, environmental effects, safety and cost. A thorough analysis and comparison between the subcritical and supercritical modes of the power loop of the system has been performed as well. Based on the proposed criteria of the working fluid selection and the simulation results, it was found that:

- Refrigerants, R717, R1234yf, and R1234ze are selected as suitable working fluids. R717 has better performance and lower cost with toxicity as main drawback. R1234yf and R1234ze have zero ODP with very low GWP and comparable performance and size with other refrigerants.
- For the cooling loop, R32, R717, and R1234yf are considered as proper fluids based on the applied criteria. R32 shows better performance.
- The size of the system is affected by the environmental and design conditions. At the same environmental conditions, the size of the pistons does not affect the power efficiency and the COP of the system. In other words, if the mass flow rate was changed by changing the ECU diameters, the performance indicators of the system remain the same.
- The subcritical mode of the system is more efficient and more compact than the supercritical mode at heat source temperature less than 90 °C. At temperatures higher than 95 °C, the supercritical mode is more efficient than the subcritical mode.

Declaration of Competing Interest

The authors declare that they have no known competing financial interests or personal relationships that could have appeared to influence the work reported in this paper.

Acknowledgment

The work presented in this publication was made possible by NPRP-S grant # [11S-1231–170155] from the Qatar National Research Fund (a member of Qatar Foundation). The findings herein reflect the work, and are solely the responsibility, of the authors.

The authors acknowledge the efforts of Mr. Maxim Glushenkov in designing the Expander-Compressor Unit.

References

Danfoss, “Refrigerant Options Now and In the Future,” no. August 2012.
Naimaster, E.J., Sleiti, A.K., 2013. Potential of SOFC CHP systems for energy-efficient commercial buildings. Energy Build. 61. doi:10.1016/j.enbuild.2012.09.045.
Sleiti, A.K., Naimaster, E.J., 2016. Application of fatty acid based phase-change material to reduce energy consumption from roofs of buildings. J. Sol. Energy Eng. Trans. ASME 138 (5). doi:10.1115/1.4033574.
Sleiti, A.K., Al-Ammaria, W.A., Al-Khawaja, M., 2020. A novel solar integrated distillation and cooling system - design and analysis. Sol. Energy 206, 68–83. doi:10.1016/j.solener.2020.05.107.
Elbeih, M., Sleiti, A.K., 2020. Analysis and optimization of concentrated solar power plant for application in arid climate. J. Energy Sci. Eng. ISSN 2050-0505, no. In productionESE-2020-01-0043.
Iir, T., Notes, I., Note, T.I., Coulomb, D., Dupont, J., 1963. The role of refrigeration in the economy. Vacuum 13 (5), 210. doi:10.1016/0042-207x(63)90508-6.
Sleiti, A.K., 2017. Tidal power technology review with potential applications in Gulf Stream. Renew. Sustain. Energy Rev. doi:10.1016/j.rser.2016.11.150.
Sleiti, A.K., Al-Ammaria, W.A., Al-Khawaja, M., 2020. Review of innovative approaches of thermo-mechanical refrigeration systems using low grade heat. Int. J. Energy Res. doi:10.1002/er.5556, no. In Production.
Lazzarin, R.M., 2014. Solar cooling: PV or thermal? A thermodynamic and economical analysis. Int. J. Refrig. doi:10.1016/j.ijrefrig.2013.05.012.
Söylemez, E., Alpman, E., Onat, A., 2018. Experimental analysis of hybrid household refrigerators including thermoelectric and vapour compression cooling systems. Int. J. Refrig. 95, 93–107. doi:10.1016/j.ijrefrig.2018.08.010.
Berdasco, M., Vallès, M., Coronas, A., 2019. Thermodynamic analysis of an ammonia/water absorption–resorption refrigeration system. Int. J. Refrig. 103, 51–60. doi:10.1016/j.ijrefrig.2019.03.023.
Habib, K., Saha, B.B., Chakraborty, A., Koyama, S., Srinivasan, K., 2011. Performance evaluation of combined adsorption refrigeration cycles. Int. J. Refrig. 34 (1), 129–137. doi:10.1016/j.ijrefrig.2010.09.005.
Jeong, J., Kang, Y.T., 2004. Cycle of a refrigeration cycle driven by refrigerant steam turbine. Int. J. Refrig. 27 (1), 33–41. doi:10.1016/S0140-7007(03)00101-4.
Rostamnejad, H., Zare, V., 2019. Performance improvement of ejector expansion refrigeration cycles employing a booster compressor using different refrigerants: thermodynamic analysis and optimization. Int. J. Refrig. 101, 56–70. doi:10.1016/j.ijrefrig.2019.02.031.
Salhi, K., Korichi, M., Ramadan, K.M., 2018. Thermodynamic and thermo-economic analysis of compression–absorption cascade refrigeration system using low-GWP HFO refrigerant powered by geothermal energy. Int. J. Refrig. 94, 214–229. doi:10.1016/j.ijrefrig.2018.03.017.
Khaliq, A., 2015. A theoretical study on a novel solar based integrated system for simultaneous production of cooling and heating. Int. J. Refrig. 52, 66–82. doi:10.1016/j.ijrefrig.2014.12.013.
Zeyghami, M., Goswami, D.Y., Stefanakos, E., 2015. A review of solar thermo-mechanical refrigeration and cooling methods. Renew. Sustain. Energy Rev. doi:10.1016/j.rser.2015.07.011.
Shestopalov, K.O., Huang, B.J., Petrenko, V.O., Volovyk, O.S., 2015. Investigation of an experimental ejector refrigeration machine operating with refrigerant R245fa at design and off-design working conditions. Part 1. Theoretical analysis. Int. J. Refrig. 55, 201–211. doi:10.1016/j.ijrefrig.2015.01.016.
Shestopalov, K.O., Huang, B.J., Petrenko, V.O., Volovyk, O.S., 2015. Investigation of an experimental ejector refrigeration machine operating with refrigerant R245fa at design and off-design working conditions. Part 2. Theoretical and experimental results. Int. J. Refrig. 55, 212–223. doi:10.1016/j.ijrefrig.2015.02.004.
Van Nguyen, V., Varga, S., Soares, J., Dvorak, V., Oliveira, A.C., 2020. Applying a variable geometry ejector in a solar ejector refrigeration system. Int. J. Refrig. 113, 187–195. doi:10.1016/j.ijrefrig.2020.01.018.
Yan, J., Lin, C., Cai, W., Chen, H., Wang, H., 2016. Experimental study on key geometric parameters of an R134A ejector cooling system. Int. J. Refrig. doi:10.1016/j.ijrefrig.2016.04.001.
Wu, H., Liu, Z., Han, B., Li, Y., 2014. Numerical investigation of the influences of mixing chamber geometries on steam ejector performance. Desalination 353, 15–20. doi:10.1016/j.desal.2014.09.002.
Foroozesh, F., Khoshnevis, A.B., Lakzian, E., 2020. Improvement of the wet steam ejector performance in a refrigeration cycle via changing the ejector geometry by a novel EEC (entropy generation, entrainment ratio, and coefficient of performance) method. Int. J. Refrig. 110, 248–261. doi:10.1016/j.ijrefrig.2019.11.006.
Dennis, M., Garzoli, K., 2011. Use of variable geometry ejector with cold store to achieve high solar fraction for solar cooling. Int. J. Refrig. 34 (7), 1626–1632. doi:10.1016/j.ijrefrig.2010.08.006.
Zhu, L., Yu, J., Zhou, M., Wang, X., 2014. Performance analysis of a novel dual-nozzle ejector enhanced cycle for solar assisted air-source heat pump systems. Renew. Energy doi:10.1016/j.renene.2013.10.030.
Roman, R., Hernandez, J.I., 2011. Performance of ejector cooling systems using low ecological impact refrigerants. Int. J. Refrig. doi:10.1016/j.ijrefrig.2011.03.006.
Nemati, A., Nami, H., Yari, M., 2017. Comparaison des frigorigènes dans un cycle frigorifique transcritique à éjecteur-détente bi-étagé, basé sur une analyse environnementale et exergo-économique. Int. J. Refrig. 84, 139–150. doi:10.1016/j.ijrefrig.2017.09.002.
Chen, Z., Jin, X., Dang, C., Hihara, E., 2017. Ejector performance analysis under overall operating conditions considering adjustable nozzle structure. Int. J. Refrig. 84, 274–286. doi:10.1016/j.ijrefrig.2017.08.005.
Yu, J., Li, Y., 2007. A theoretical study of a novel regenerative ejector refrigeration cycle. Int. J. Refrig. 30 (3), 464–470. doi:10.1016/j.ijrefrig.2006.08.011.
Srisastra, P., Aphornratana, S., Sriveerakul, T., 2008. Development of a circulating system for a jet refrigeration cycle. Int. J. Refrig. 31 (5), 921–929. doi:10.1016/j.ijrefrig.2007.09.002.
Sanaye, S., Refahi, A., 2020. A novel configuration of ejector refrigeration cycle coupled with organic Rankine cycle for transformer and space cooling applications. Int. J. Refrig. 115, 191–208. doi:10.1016/j.ijrefrig.2020.02.005.
Sioud, D., Bourouis, M., Bellagi, A., 2019. Investigation of an ejector powered double-effect absorption/recompression refrigeration cycle. Int. J. Refrig. 99, 453–468. doi:10.1016/j.ijrefrig.2018.11.042.
Heidari, A., Rostamzadeh, H., Avami, A., 2019. A novel hybrid desiccant-based ejector cooling system for energy and carbon saving in hot and humid climates. Int. J. Refrig. 101, 196–210. doi:10.1016/j.ijrefrig.2019.03.028.
Ziviani, D., Groll, E.A., Braun, J.E., De Paepe, M., 2018. Review and update on the geometry modeling of single-screw machines with emphasis on expanders. Int. J. Refrig. 92, 10–26. doi:10.1016/j.ijrefrig.2018.05.029.
Frutiger, J., et al., 2016. Working fluid selection for organic Rankine cycles - Impact

of uncertainty of fluid properties. Energy 109, 987–997. doi:10.1016/j.energy.2016.05.010.

Sleiti, A.K., Al-Ammari, W.A., Al-Khawaja, M., 2020. Review of innovative approaches of thermo-mechanical refrigeration systems using low grade heat. Int. J. Energy Res. doi:10.1002/er.5556.

Sleiti, A.K., Rasras, A., Jafar, W., Alam, M., Glushenkov, M., Kronberg, A., 2018. Novel thermo mechanical refrigeration cycle utilizing waste heat. Elev. Int. Conf. Therm. Eng. Theory Appl. (2018) 1–5. 2018, no. Vol 2018ICTEA 2018 https://caos.library.ryerson.ca/index.php/ictea/article/view/243 .

Glushenkov, M., Kronberg, A., Knoke, T., Kenig, E.Y., 2018. Isobaric expansion engines: new opportunities in energy conversion for heat engines, pumps and compressors. Energies 11 (1). doi:10.3390/en11010154.

ASME, "Worthington Direct-Acting Simplex Steam Pump from the USS Monitor." USS Monitor Center at The Mariners' Museum and Park Newport News, Virginia, Newport, 2016.

Duarte, W.M., Paulino, T.F., Pabon, J.J.G., Sawalha, S., Machado, L., 2019. Refrigerants selection for a direct expansion solar assisted heat pump for domestic hot water. Sol. Energy 184 (April), 527–538. doi:10.1016/j.solener.2019.04.027.

Aphornratana, S., Sriveerakul, T., 2010. Analysis of a combined Rankine-vapour-compression refrigeration cycle. Energy Convers. Manag. 51 (12), 2557–2564. doi:10.1016/j.enconman.2010.04.016.

Airmax pneumatics LTD, *How 3/2 Way Single Pilot Valve Works*. YouTube, 2020.

Bianchi, M., De Pascale, A., 2011. Bottoming cycles for electric energy generation: parametric investigation of available and innovative solutions for the exploitation of low and medium temperature heat sources. Appl. Energy doi:10.1016/j.apenergy.2010.11.013.

Hammond, G.P., Norman, J.B., 2014. Heat recovery opportunities in UK industry. Appl. Energy 116, 387–397. doi:10.1016/j.apenergy.2013.11.008.

Heberle, F., Brüggemann, D., 2015. Thermo-economic evaluation of organic rankine cycles for geothermal power generation using zeotropic mixtures. Energies 8 (3), 2097–2124. doi:10.3390/en8032097.

Chen, H., Goswami, D.Y., Stefanakos, E.K., 2010. A review of thermodynamic cycles and working fluids for the conversion of low-grade heat. Renew. Sustain. Energy Rev. 14 (9), 3059–3067. doi:10.1016/j.rser.2010.07.006.

Cengel, Y.A., Boles, M.A., 2015. Thermodynamics: An Engineering Approach, 8th edition, McGraw-Hill Education.